Supplement of Clim. Past, 13, 1527–1537, 2017
https://doi.org/10.5194/cp-13-1527-2017-supplement

Climate of the Past
Open Access

Supplement of

Episodic Neoglacial expansion and rapid 20th century retreat of a small ice cap on Baffin Island, Arctic Canada, and modeled temperature change

Simon L. Pendleton et al.

Correspondence to: Simon L. Pendleton (simon.pendleton@colorado.edu)

Supplemental Information

1. Alternative Time-Distance Plot

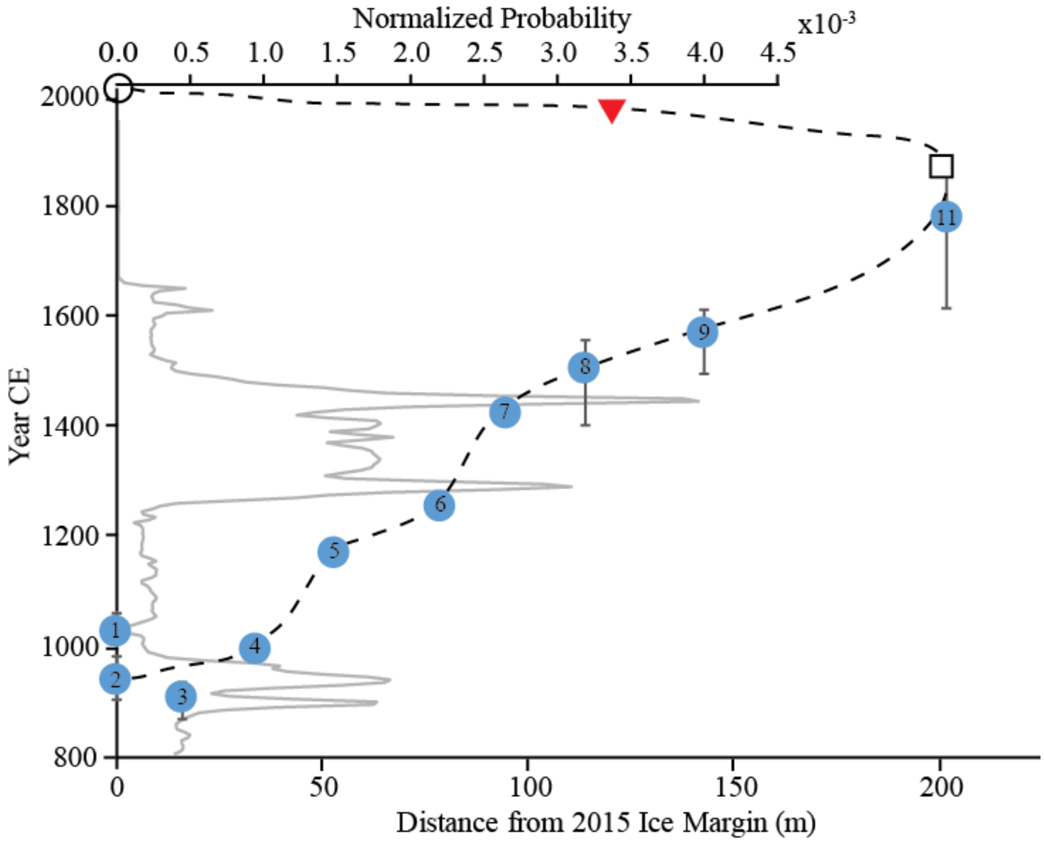

Figure S1: An alternative view of manuscript Figure 3. The same transect radiocarbon ages are show here in a Time vs. Distance away from 2015 Ice margin. All other aspects of the figure are the same as main manuscript Figure 3.

2. Ice Margin *In situ* Plant ages

Compiled samples from Miller et al. (2013) and Margreth et al. (2014) for the past 2 ka (from manuscript Figure 3)

Field ID	Latitude	Longitude	Elevation (m)	^{14}C age (yr)	^{14}C ± (yr)	Cal. BP Age (1950)*	Uncertainty (-yr)	Uncertainty (+yr)
09SRB-E265A-01	66.1052081	-64.587198	1037	155	20	158	-149	116
09SRB-K047A-01	66.2154431	-64.370017	959	165	25	160	-154	121
09SRB-K051A-01	66.2483348	-64.272212	1045	185	20	167	-167	116
09SRB-K048A-01	66.2186164	-64.357094	998	165	15	168	-159	107
09SRB-K064A-01	66.1067164	-64.337882	956	200	20	170	-170	118
M09-B107v	71.04155	-74.66817	852	1215	25	211	-57	86
09SRB-E263A-01	66.1152081	-64.569872	939	245	30	256	-103	52
09SRB-E266A-01	66.0965965	-64.589275	1014	255	25	287	-130	22
09SRB-E263A-01	66.1152081	-64.569872	939	255	15	290	3	15
05SRP-17	71.495039	-77.478825	780	275	15	336	-39	82
M10-B032V	70.90233	-73.25257	1118	310	20	381	-73	47
05SRP-59	71.49829	-77.51784	738	315	15	382	-71	45
M10-B204V	72.96828	-82.79733	872	345	20	395	-75	66
05TGR-19	71.40865	-78.77593	663	355	20	403	-73	72
05SRP-57B	71.5443	-77.3263	900	360	15	411	-78	64
09SRB-K098A-01	66.1951148	-64.203042	1199	365	20	415	-82	68
09SRB-Q013A-01	66.2899331	-64.037932	1000	385	25	437	-102	63
05ORN-50	71.5246	-77.96909	797	390	15	463	5	35
09SRB-K073A-01	65.7925798	-63.943137	877	405	25	465	2	40
09SRB-E264A-01	66.1103081	-64.581673	970	405	20	475	1	29
09SRB-K094A-01	66.2106964	-64.190795	1309	405	20	475	1	29
05SRP-39	71.51572	-77.44729	742	400	15	478	0	23
05PL-02	71.60063	-78.4621	767	410	15	489	-4	14
M09-B120v	71.07193	-74.69194	778	410	15	489	-4	14
05ORN-57	71.51777	-77.97078	804	435	15	503	-4	6
05ORN-17	71.56608	-78.09187	815	440	15	505	-4	6
05SRP-57A	71.54432	-77.32632	900	445	20	506	-5	8
M09-B089v	71.01734	-74.8122	727	450	20	508	-6	7
05SRP-27	71.50665	-77.48801	748	450	15	509	-6	4
05SRP-47	71.51874	-77.39766	867	450	15	509	-6	4
M09-B090v	71.01851	-74.8172	727	460	15	512	-6	4
M81-BM6b	71.31811	-78.71281	660	460	25	512	-8	8
05SRP-16B	71.47535	-77.51295	797	465	15	513	-6	5
05SRP-24	71.49965	-77.44927	845	480	15	518	-7	5
05SRP-52A	71.52339	-77.3551	874	480	20	519	-9	6
05ORN-43	71.53951	-77.97321	781	505	15	526	-6	7
M10-B198V	73.19093	-82.32833	881	510	15	528	-6	7
05SRP-29	71.50941	-77.50816	696	530	20	542	-17	2
05ORN-59	71.51777	-77.97078	804	550	15	563	-29	54
M09-B093v	71.05914	-74.72184	904	550	20	568	-35	52
05SRP-58	71.52009	-77.398027	863	560	15	577	-38	44
M09-B041V	71.45258	-77.47724	766	560	20	580	-42	43
05SRP-56	71.53867	-77.323176	885	565	15	583	-42	39
M09-B227v	71.79554	-76.60952	1066	565	15	583	-42	39

*Radiocarbon dates were calibrated using OxCal 4.2.4 (Bronk-Ramsey, 2009; Reimer et al., 2013)

2.1. *In situ* Plant Ages (cont.)

Field ID	Latitude	Longitude	Elevation (m)	^{14}C age (yr)	^{14}C ± (yr)	Cal. BP Age (1950)*	Uncertainty (-yr)	Uncertainty (+yr)
05ORN-54	71.51621	-77.95787	782	575	15	592	-47	33
05SRP-26	71.50126	-77.45674	833	575	15	592	-47	33
05TGR-26	71.4064	-78.82849	738	585	20	597	-48	34
05SRP-52B	71.52339	-77.3551	874	590	15	599	-47	32
M10-B210V	72.2462	-79.12092	840	590	15	599	-47	32
05SRP-54	71.53457	-77.33562	880	595	15	601	-48	34
05ORN-56B	71.51511	-77.96629	793	600	15	602	-48	36
05TGR-01	71.31821	-78.70509	629	600	15	602	-48	36
05ORN-20	71.5614	-78.06895	763	605	15	603	-47	39
05ORN-44	71.53889	-77.97203	778	605	15	603	-47	39
05SRP-61	71.49398	-77.54775	750	610	15	604	-47	40
M09-B142v	70.90735	-73.61873	998	610	15	604	-47	40
05PL-04	71.60063	-78.4621	767	615	15	604	-46	42
05SRP-66	71.48789	-77.5524	774	615	15	604	-46	42
05TGR-09	71.377568	-78.761183	746	620	15	605	-46	43
05ORN-62	71.52676	-77.994947	818	625	15	605	-44	45
09SRB-K092A-01	66.2037314	-64.178252	1153	625	15	605	-44	45
05TGR-27	71.40521	-78.82803	737	645	20	608	-43	49
M09-B125v	71.0746	-74.67576	680	645	20	608	-43	49
M09-B104v	71.06007	-74.71937	917	655	15	611	-43	49
05ORN-61	71.52076	-77.98561	799	660	15	615	-46	46
M09-B016V	71.51554	-76.53301	874	665	20	619	-50	45
M09-B108v	71.04024	-74.65705	829	665	20	619	-50	45
05ORN-39	71.54166	-78.00658	868	680	25	631	-60	39
M10-B024V	70.84775	-73.4823	1007	675	15	634	-60	33
M09-B099v	71.062	-74.71164	929	680	20	635	-62	34
M09-B059V	70.97187	-74.7337	696	685	20	642	-67	29
M09-B100v	71.06192	-74.71189	928	690	20	648	7	24
05ORN-13	71.58298	-78.16529	829	685	15	649	7	20
05TGR-13	71.38353	-78.74943	708	690	15	655	3	14
09SRB-K059A-01	66.1126931	-64.265394	1025	715	20	669	-4	8
M09-B127v	71.07698	-74.67796	661	715	15	670	-4	5
05ORN-38	71.54292	-78.02479	892	725	15	674	-5	4
09SRB-K074A-01	65.7961098	-63.944114	924	750	20	684	-11	4
M10-B193V	73.2208	-81.98243	813	755	20	686	-12	4
M09-B140v	70.98071	-73.66206	1143	765	15	690	-13	3
05ORN-23	71.5544	-78.06365	790	780	15	700	-18	22
09SRB-K058A-01	66.1088498	-64.260797	1066	845	20	751	-20	29
05ORN-09	71.58835	-78.1943	825	880	25	800	-60	91
M09-B141v	70.98064	-73.66207	1144	915	15	852	-59	50
05ORN-34	71.54297	-78.02676	894	930	20	853	-55	55
M10-B167V	72.25617	-77.29832	1145	930	20	853	-55	55
05ORN-10	71.58835	-78.1943	825	940	15	853	-53	59
M10-B174V	72.24443	-78.14567	1052	1050	20	954	-19	7

*Radiocarbon dates were calibrated using OxCal 4.2.4 (Bronk-Ramsey, 2009; Reimer et al., 2013)

3. Calibration of Solar Radiation Melt Factor

Holding all other parameters constant, the model was calibrated for a range of *mR* values using the observed transect chronology. Given the asymmetry of the Holocene maximum extent (LIA) trimlines, there should be a small range of *mR* values that can reproduce the observed ice cap dimensions (Fig. S2).

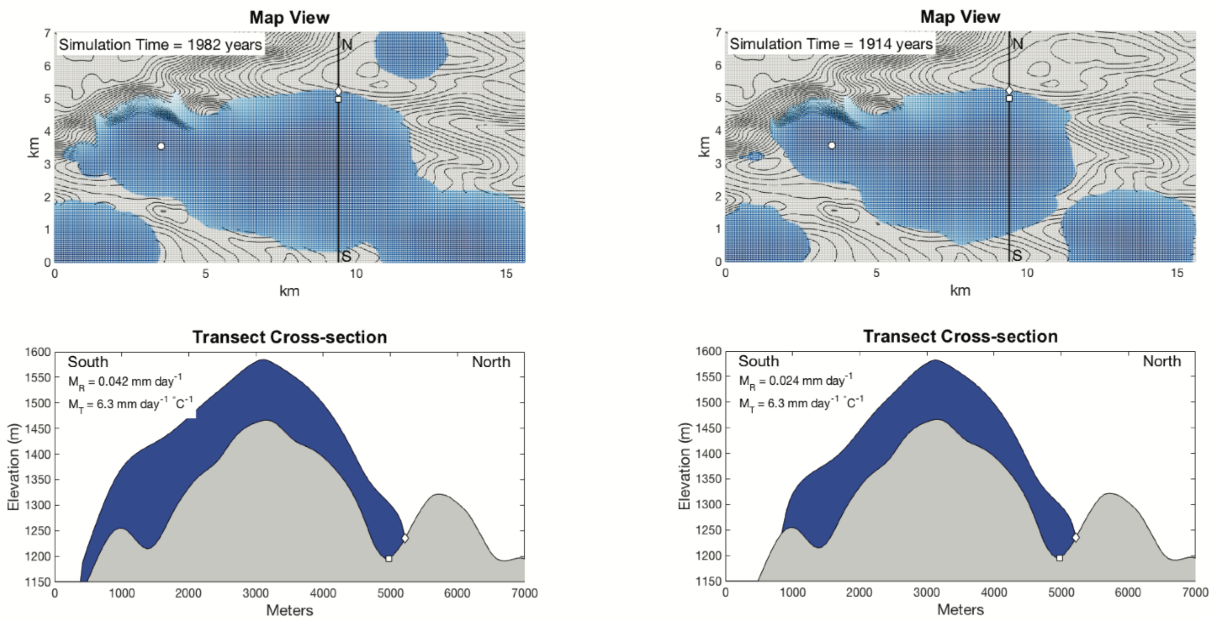

Figure S2: Results of the solar radiation melt factor calibration showing that, with all other parameters held constant, *mR* values above and below 0.036 mm day^{-1} produce too much (left panel) or too little (right panel) ice, respectively, over the course of the simulation.

4. Glacier Model Sensitivity Analysis

Among the parameter values prescribed for this model, the uniform and constant accumulation rate is perhaps the most uncertain and therefore could have the largest impact on the model outcome. To test model sensitivity to accumulation rate, we ran the model to completion as above using 0.2 and 0.5 m.w.e. (meters water equivalent). Keeping all other parameters the same, including the solar radiation melt factor calibrated form the original run, simulations with 0.5 m.w.e. fail to reproduce the correct LIA ice configuration. This is partly due to the fact that a higher accumulation rate has a higher equilibrium line altitude (ELA) and necessitates a warmer mean annual temperature than the original scenario to accumulate snow/ice at the same elevations (the same temperature forcing with a higher accumulation rate would produce too much ice and covers the entire study area). This higher temperature increases the length of the melt season (Fig. S3), therefore amplifying the influence of the solar radiation melt factor (which is only in effect when air temperature is above 0°C).

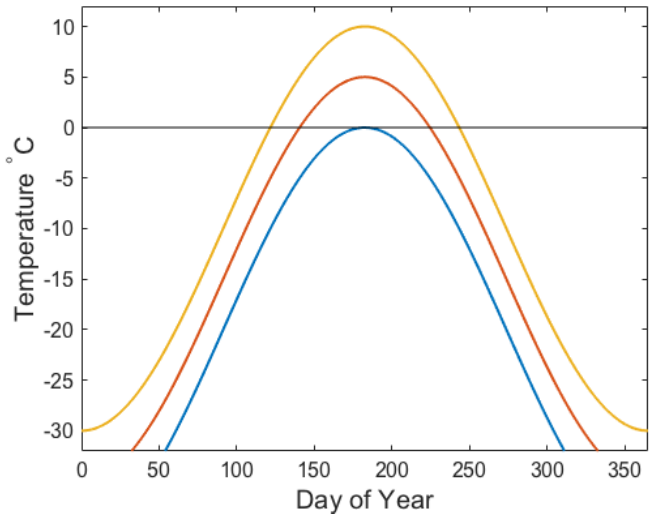

Supplemental Figure S3: Modeled daily annual temperatures illustrating the changing length of melt season (portion of curve above 0°C) with changing mean annual temperature.

This then amplifies the asymmetry of ice distribution and prevents ice from advancing through the transect chronology as observed. However, when the solar melt factor is lowered to compensate for the above increase in melt season length, the only way to advance ice through the chronology in the observed time constraints is to raise temperatures during the 2nd millennium CE and through the LIA, which itself it highly unlikely. Additionally, the Holocene maximum extent from these higher accumulation and lower solar melt factor runs deviate greatly from the observed maximum extent (Fig. S4).

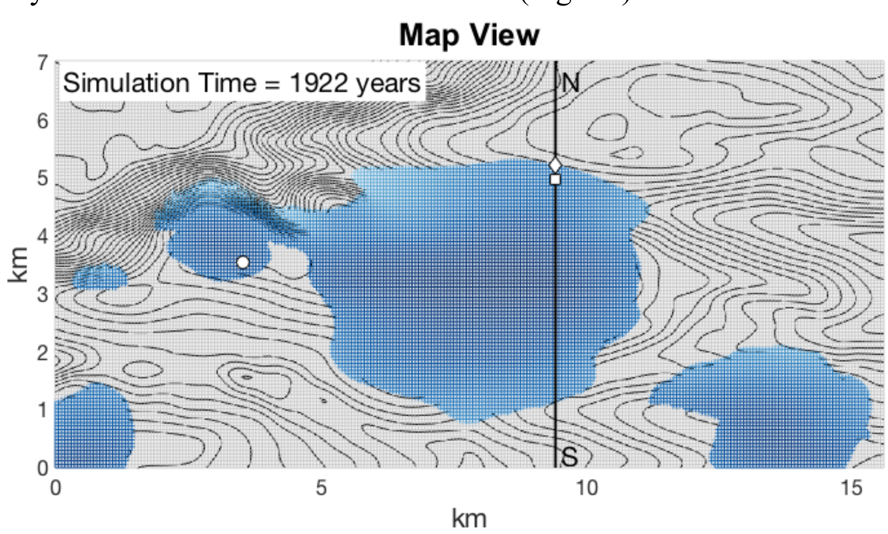

Supplemental Figure S4: Maximum Holocene extent under higher accumulation rate and lower solar radiation melt factor illustrating highly asymmetric configuration deviating from observed maximum extent (manuscript Figure 2). Also show are the locations of sample #12 (circle), 1000CE margin (square), and LIA limit (diamond).

These results from the higher accumulation scenario suggest that indeed the accumulation rate at the study site is likely less than 0.5 m.w.e.

Conversely, a lower accumulation rate of 0.2 m.w.e. raises the ELA and thus requires slightly cooler temperatures to accumulate ice at the correct elevations. When run with the same parameter values as the original simulation we find that total minimum required cooling over the last ~2000 years increases from 0.45 to 0.5°C. This makes sense, since less accumulation would raise the ELA, then a temperature decrease is needed to lower it again. However, since cooler mean annual temperatures shorten the melt season, and lessening the influence of solar melt, model simulations with a lower accumulation rate have less asymmetry in the final ice configuration, and thus deviating from the observed Holocene maximum ice configuration (Fig. S5).

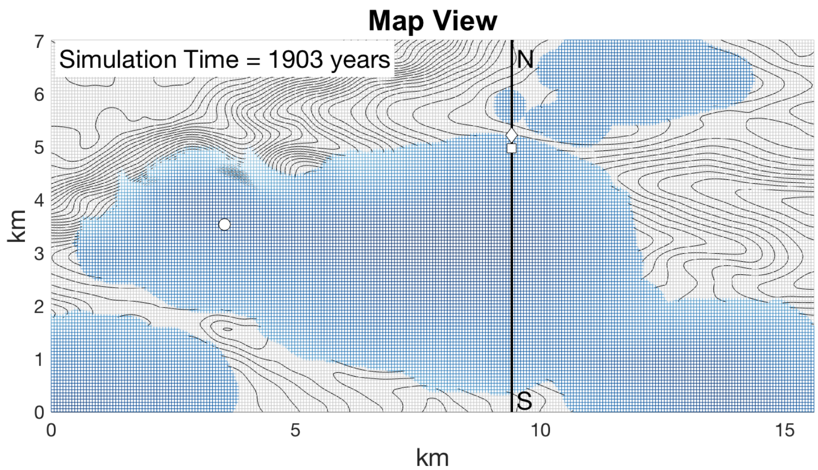

Figure S5: Modeled Holocene maximum extent using a lower accumulation and same solar radiation melt factor as LIA simulation in manuscript (Figure 4). Note lack of ice cap asymmetry which fails to match the observed maximum extent.

5. Glacier Model Uncertainty

In the modeling experiments used in this study, uncertainty is difficult to quantify, but it is worthwhile to acknowledge potential sources of error and uncertainty. First, though modeled ice thicknesses agreed with the thickness of modern ice removed to create an unglaciated surface, collection of subglacial topography data would greatly reduce the error here.

Second, sensitivity analysis showed that the accumulation rate is likely fairly accurate, however, longer term records of accumulation in the region would help to reduce uncertainty with the mass balance. Additionally, in situ mass balance data, including incoming solar radiation would allow for the calibration of a local solar radiation melt factor (e.g., Jonsell et al., 2012).

Third, super imposed ice (or refrozen melt water) is thought to be an important component of mass balance, especially for polar glaciers. However, even though refrozen melt water can account for up to ~20% of annual accumulation (Wadham and Nuttall, 2002), it can vary significantly due to percolation and drainage flow paths (Cuffey and Paterson, 2010). (Zwinger and Moore, 2009) used in situ observation data to attempt to capture the effect of refreeze both in terms of accumulation and heat transfer. However, lacking any such data for DIC, attempting to model such a process would only introduce additional assumptions and uncertainty. Field observations of the ice cap showed numerous supraglacial meltwater channels and no obvious signs of large scale refreeze, suggesting that DIC may shed meltwater efficiently, reducing the impact of super imposed ice.

Additionally, wind redistribution of snow likely plays a part in the mass balance of Divide Ice cap and the asymmetry present in the Holocene maximum extent. Capturing this factor is beyond the scope of this study, but important to acknowledge. The model in this study captures the first-order trends and highlights areas of where similar future studies could benefit from additional observation and measurements to reduce error and improve model performance.

References

Cuffey, K. M. and Paterson, W. S. B.: The physics of glaciers, Fourth ed., Academic Press, Kidlington, UK., 2010.

Jonsell, U., Navarro Valero, F. J., Bañón, M., Izargain, L., Jesús, J. and Otero García, J.: Sensitivity of a distributed temperature-radiation index melt model based on AWS observations and surface energy balance fluxes, Hurd Peninsula glaciers, Livingston Island, Antarctica, Cryosph., 6(3), 539–552, 2012.

Margreth, A., Dyke, A. S., Gosse, J. C. and Telka, A. M.: Neoglacial ice expansion and late Holocene cold-based ice cap dynamics on Cumberland Peninsula, Baffin Island, Arctic Canada, Quaternary Sci. Rev., 91, 242–256, doi:10.1016/j.quascirev.2014.02.005, 2014.

Miller, G. H., Lehman, S. J., Refsnider, K. A., Southon, J. R. and Zhong, Y.: Unprecedented recent summer warmth in Arctic Canada, Geophys. Res. Lett., 40(21), 5745–5751, 2013.

Wadham, J. L. and Nuttall, A. M.: Multiphase formation of superimposed ice during a mass-balance year at a maritime high-Arctic glacier, J. Glaciol., 48(163), 545–551, doi:10.3189/172756502781831025, 2002.

Zwinger, T. and Moore, J. C.: Diagnostic and prognostic simulations with a full Stokes model accounting for superimposed ice of Midtre Lovénbreen, Svalbard, Cryosph., 3, 217–229, doi:10.5194/tc-3-217-2009, 2009.